AIAA AVIATION Forum
17-21 June 2019, Dallas, Texas
AIAA Aviation 2019 Forum

10.2514/6.2019-2953

Optimization of Diagonal-Norm Multidimensional Summation-by-Parts Operators on Simplices

André L. Marchildon* and David W. Zingg†
University of Toronto Institute for Aerospace Studies, Toronto, Ontario, M3H 5T6

Finite-difference summation-by-parts (SBP) operators have recently been extended to non-tensor-product multidimensional elements, thus allowing operators to be constructed on elements such as simplices. In the construction of multidimensional SBP operators there are often free parameters that can be used to optimize the operators. This work introduces methods to construct SBP operators using the minimum number of degrees of freedom such that the remaining free parameters can be used to optimize the operators. This includes constructing the cubature rules required for the SBP operators algebraically rather than numerically such that the influence of the nodal locations and cubature weights on the SBP operators can be investigated. The free parameters are used to meet objective functions such as minimizing the element integration error, the Frobenius norm, the leading truncation term, or combinations of these objective functions. The linear convection equation is solved with SBP operators constructed on three-dimensional simplex elements to study the impact of optimizing the free parameters for these various objective functions on the solution error. The results demonstrate that increasing the degree of the cubature rule from $2p-1$ to $2p$, where p is the degree of the operator, is beneficial at reducing the solution error even when the operator has additional nodes and is more computationally expensive. However, the results indicate that increasing the degree of the cubature rule from $2p$ to $2p+1$ does not provide a similar benefit.

I. Introduction

Finite-difference summation-by-parts (SBP) operators are actively being researched for solving linear and non-linear partial differential equations. In the field of aerodynamics for example, SBP operators have been used in aerodynamic shape optimization of unconventional aircraft configurations [1, 2]. The attractive properties of SBP operators are their robustness, provable stability, and straightforward extension to higher order [3]. SBP operators are provably stable for linear problems thanks to their construction that allows them to discretely mimic integration-by-parts. Proving stability of SBP operators for non-linear problems has also been shown by using entropy stability [4]. While SBP operators with diagonal and dense-norm matrices have been derived, only the former has been proven stable for curvilinear grids [5]. Consequently, SBP operators with diagonal-norm matrices are more commonly considered [3]. The extension to higher order is beneficial since some problems have been shown to be solved more efficiently with higher-order methods [6–9]. The mesh interface and boundary conditions for SBP operators are typically applied using simultaneous approximation terms (SATs) that weakly enforce the boundary conditions and require only C^0 continuity across block interfaces.

The construction of one-dimensional SBP operators was extended by Del Rey Fernández *et al.* to so called generalized SBP operators [10] to allow for operators with non-uniform nodal distributions, with or without nodes on the boundaries, and for non-repeating interior stencils. To extend SBP operators to two and three dimensions, tensor-products have previously been used [11, 12]. The extension of SBP operators to multiple dimensions that are not based on tensor-products was presented by Hicken *et al.* [13] as well as Del Rey Fernández *et al.* [14].

SBP operators of degree p are required to have a norm matrix that holds exclusively positive weights for a cubature rule of degree at least $2p-1$ [15]. Cubature rules in one dimension, commonly referred to as quadrature rules, have been extensively studied. For example, the Legendre-Gauss quadrature rule can be generated algebraically and is known to exactly integrate polynomials of the highest possible degree for a given number of nodes [16]. Liu and Vinokur [17] derived a set of equations to algebraically derive cubature rules with degrees of up to five for symmetrically located

*M.A.Sc Student, Institute for Aerospace Studies, 4925 Dufferin Street (andre.marchildon@mail.utoronto.ca).
†University of Toronto Distinguished Professor of Computational Aerodynamics and Sustainable Aviation, Director, Centre for Research in Sustainable Aviation, Director, Centre for Computational Science and Engineering, Institute for Aerospace Studies, 4925 Dufferin Street, and AIAA Associate Fellow (dwz@oddjob.utias.utoronto.ca).

nodes in simplex elements of one, two and three dimensions. With these equations, Liu and Vinokur derived cubature rules of a given degree with the minimum number of nodes. Additionally, Liu and Vinokur noted that many previously published cubature rules could be found using their equations and setting the free parameters to a given value. However, the equations that need to be solved for cubature rules are non-linear and get progressively more complicated as cubature rules of higher degree are sought. Most cubature rules for triangles and tetrahedra have instead been found numerically with an objective function that requires the error of the numerical integration of all polynomials of a given degree to be less than a small set tolerance [18–21].

Unlike finite-element methods, which often have separate interpolation and cubature nodes, SBP operators usually have only one set of nodes. Unfortunately, the requirements for good interpolation nodes are different than for cubature nodes. For example, equidistant nodes are used to generate the Newton-Cotes quadrature rule. However, equidistant nodes are undesirable interpolation nodes since they are susceptible to the Runge phenomenon. Furthermore, valid cubature rules, and by extension valid SBP operators, of a desired degree could be generated with all the nodes arbitrarily close together. However, these nodes would not be good interpolation nodes since they would not be representative of the solution across the entire element. A good indicator of the quality of a set of interpolation nodes is the Lebesgue constant, which bounds the interpolation error using the infinity norm [22]. It can be shown that maximizing the determinant of the Vandermonde matrix evaluated at the interpolation nodes reduces the size of the Lebesque constant [22]. The nodes that maximize the Vandermonde matrix are called Fekete nodes and in one dimension they are known to be the Legendre-Gauss-Lobatto quadrature nodes [23].

The impact of the nodal locations for flux reconstruction schemes, which only use one set of nodes like SBP schemes, with triangular elements was investigated by Witherden and Vincent [24]. The requirements for the cubature rules included having a unisolvent point set, the nodes symmetrically located in the element and for the number of nodes to match the cardinality of the basis for the degree of the operator. With these criteria, hundreds of cubature rules were generated and the flux reconstruction operators were constructed. The two-dimensional Euler equations were solved for an isentropic Euler vortex problem. The operators for degrees three to seven that had the lowest average and final L^2 error were found to have both a low Lebesque constant and a low integration error for basis functions one degree higher than were integrated exactly. A similar study was performed for flux reconstruction schemes with tetrahedral elements by Witherden *et al.* [25]. The Euler equations were solved for two test cases: a manufactured sinusoidal solution and an isentropic Euler vortex. Witherden *et al.* found that the cubature rule that had the lowest final L^2 error for one test case did not have the best result for the other test case. This indicated that optimizing the operator for one test case does not necessarily provide the ideal operator for all cases.

In the construction of one-dimensional SBP operators there are free parameters that have been used to optimize for various objective functions such as minimizing the truncation error, the spectral radius, the bandwidth, or combinations of these objectives [26, 27]. Mattsson *et al.* [27] optimized the nodal locations for three boundary nodes as well as the free parameters gained by adding additional boundary stencils in order to minimize the norm of the leading truncation error. The optimized operators were found to have a solution error an order of magnitude smaller than the one-dimensional operators constructed with all equidistant nodes and the minimum number of boundary stencils. The optimization of free parameters in the construction of multidimensional SBP operators has not previously been considered. The objective of the current work is to investigate how free parameters in the construction of multidimensional SBP operators with diagonal-norm matrices can be used to optimize the operators. A review of the construction of multidimensional SBP operators and of symmetrical cubature rules is provided in Section II. The following section shows how the SBP operators can be constructed such that they have free parameters that can be used to optimize them. The objective functions and the test case that are used to evaluate the optimized SBP operators are presented in Section IV. Sections V, VI and VII present the results for the optimized operators.

II. Review of multidimensional summation-by-parts operators

The notation and construction of SBP operators, which is based on [14], are presented in Section II A. Three different families of SBP operators constructed on simplices are then presented in Section II B.

A. Notation and construction of summation-by-parts operators

The physical domain and its boundary are denoted by Ω and Γ, respectively, while the computational domain is denoted by $\hat{\Omega}$ and $\hat{\Gamma}$, respectively. Facets indicate edges for two-dimensional elements and faces for three dimensional elements. The coordinates for the physical space are indicated by $(x, y, z) \in \Omega$, while in the computational space they

are given by $(\xi, \eta, \zeta) \in \hat{\Omega}$. The construction of two-dimensional operators is only shown for one direction since it is analogous in the other directions. Also, it is straightforward to extend the generation of operators to three dimensions using the methodology in this section as well as the one presented in Section III.

Capital letters with a script type denote functions. For example, $\mathcal{U}(\xi) \in C^0[\xi_1, \xi_n]$ represents a continuous function from ξ_1 to ξ_n. The set of n volume nodes on which the functions and operators are discretized is given by $S_{\hat{\Omega}} = \{(\xi_i, \eta_i)\}_{i=1}^{n} \subset \hat{\Omega}$. The set of facet nodes where boundary and interface conditions are imposed pointwise is given by $S_{\hat{\Gamma}_j} = \{(\xi_i^{(j)}, \eta_i^{(j)})\}_{i=1}^{n_j}$, where j is the local facet number. A lower-case bold font is used to represent the restriction of a function to the nodes in a column vector. For example, the restriction of the k-th basis function to the nodes is written as

$$\boldsymbol{p}_k \equiv [\mathcal{P}_k(\xi_1, \eta_1), \ldots, \mathcal{P}_k(\xi_n, \eta_n)]^T,$$

and similarly, the first derivative $\frac{\partial}{\partial \xi}$ of the k-th polynomial is denoted by

$$\boldsymbol{p}_k' \equiv \left[\frac{\partial \mathcal{P}_k}{\partial \xi}(\xi_1, \eta_1), \ldots, \frac{\partial \mathcal{P}_k}{\partial \xi}(\xi_n, \eta_n)\right]^T.$$

The cardinality of polynomials of degree p is indicated by

$$N_{p,d}^* \equiv \binom{p+d}{d},$$

where d is the number of spatial dimensions. The cardinality evaluates to $N_{p,1}^* = (p+1)$, $N_{p,2}^* = (p+1)(p+2)/2$, and $N_{p,3}^* = (p+1)(p+2)(p+3)/6$. The rectangular Vandermonde matrix of degree p evaluated at the nodes is

$$\mathsf{V} = [\boldsymbol{p}_1, \ldots, \boldsymbol{p}_{N_{p,d}^*}],$$

while the ξ derivative of the polynomials evaluated at the nodes is

$$\mathsf{V}_\xi = [\boldsymbol{p}_1', \ldots, \boldsymbol{p}_{N_{p,d}^*}'].$$

We now provide the following definition for a multi-dimensional SBP operator [13]:

Definition 1. ***Two-dimensional summation-by-parts operator:*** *The matrix D_ξ is an approximation to the first derivative $\frac{\partial}{\partial \xi}$ on the nodes $S_{\hat{\Omega}}$, where $\hat{\Omega}$ is an open and bounded domain $\in \mathbb{R}^2$ with a piecewise linear boundary $\hat{\Gamma}$, if*

1) $\mathsf{D}_\xi \boldsymbol{p}_k = \boldsymbol{p}_k', \quad \forall k \in \{1, 2, \ldots, N_{p,d}^*\}$;
2) $\mathsf{D}_\xi = \mathsf{H}^{-1}\mathsf{Q}_\xi$, where H is symmetric positive-definite; and
3) $\mathsf{Q}_\xi = \mathsf{S}_\xi + \frac{1}{2}\mathsf{E}_\xi$, where $\mathsf{S}_\xi^T = -\mathsf{S}_\xi$, $\mathsf{E}_\xi^T = \mathsf{E}_\xi$, and E_ξ satisfies

$$\boldsymbol{p}_k^T \mathsf{E}_\xi \boldsymbol{p}_m = \oint_{\hat{\Gamma}} \mathcal{P}_k \mathcal{P}_m n_\xi d\hat{\Gamma}, \quad \forall k, m \in \{1, 2, \ldots, N_{r,d}^*\},$$

where n_ξ is the ξ component of the unit outward pointing normal $\boldsymbol{n} = [n_\xi, n_\eta]^T$ on $\hat{\Gamma}$ and $r \geq p$. The integer r is the degree of the interpolation/extrapolation operator R, which is presented shortly.

It is shown in [13] that a cubature rule of degree at least $2p-1$ with exclusively positive weights along with a generalized Vandermonde matrix with linearly independent columns is necessary and sufficient for a diagonal-norm SBP operator of degree p to exist that approximates the first derivative $\frac{\partial}{\partial \xi}$ and $\frac{\partial}{\partial \eta}$ on the set of nodes $S_{\hat{\Omega}}$.

Remark 1. *For one-dimensional operators, the requirement that the columns of the Vandermonde matrix need to be linearly independent is equivalent to requiring that each nodal location is unique. However, in multiple dimensions, having unique nodal locations is insufficient to ensure that the columns of the Vandermonde matrix are linearly independent [28]. Furthermore, the requirement that the columns of the Vandermonde matrix be linearly independent is similar but not as stringent as requiring a unisolvent nodal set. The latter requires that the Vandermonde matrix be invertible and thus that $n = N_{p,d}^*$, while the former allows for $n \geq N_{p,d}^*$ [13].*

The norm matrix H has exclusively positive weights and is a cubature rule satisfying

$$\boldsymbol{p}_k^T \mathsf{H} \boldsymbol{p}_m = \int_{\hat{\Omega}} \mathcal{P}_k \mathcal{P}_m d\hat{\Omega},$$

where the maximum degree of $\mathcal{P}_k\mathcal{P}_m$ is $2p-1$. Therefore, the norm matrix is also a $2p-1$ degree approximation to the L^2 norm

$$||\boldsymbol{u}||_{\mathsf{H}}^2 \equiv \boldsymbol{u}^t \mathsf{H} \boldsymbol{u} \approx \int_{\hat{\Omega}} \mathcal{U}^2 d\hat{\Omega}.$$

It is common in numerical analysis of SBP operators to quantify the error using a broken norm [29]

$$||\boldsymbol{u}||_{\mathsf{H}_g}^2 = \sum_{i=1}^{K} ||\boldsymbol{u}_i||_{\mathsf{H}}^2,$$

where K is the number of non-overlapping elements, and the norm matrix H for each element is scaled by the determinant of the appropriate mapping Jacobian. To proceed further in the construction of SBP operators we first require [13]:

Assumption 1. *The reference element $\hat{\Omega}$ is a polygon with piecewise linear boundaries $\hat{\Gamma} = \cup_{j=1}^{N_{\hat{\Gamma}}} \hat{\Gamma}_j$ and $\cap_{j=1}^{N_{\hat{\Gamma}}} \hat{\Gamma}_j = \emptyset$. Additionally, there exists a cubature rule on each $\hat{\Gamma}_j$ with nodes $S_{\hat{\Gamma}_j}$ and weights $\{b_i^{(j)}\}_{i=1}^{n_j}$ that exactly integrates all polynomials of degree $q \geq 2p$.*

To apply the boundary and interface conditions on facet j of the reference element, an interpolation/extrapolation operator of at least degree r is required to interpolate/extrapolate the solution from $S_{\hat{\Omega}}$ to $S_{\hat{\Gamma}_j}$

$$\mathsf{R}_j \mathsf{V}_{\hat{\Omega}} = \mathsf{V}_{\hat{\Gamma}_j}. \tag{1}$$

Del Rey Fernández *et al.* [14] showed that Assumption 1 ensures that the interpolation/extrapolation operator, R_j, can be constructed as

$$\mathsf{R}_j = \mathsf{V}_{\hat{\Gamma}_j} (\mathsf{V}_{\hat{\Omega}})^{\dagger}, \tag{2}$$

where $(\cdot)^{\dagger}$ indicates the Moore-Penrose pseudoinverse. The directional surface operator, E_ξ, can be constructed using the interpolation/extrapolation operator:

$$\mathsf{E}_\xi = \sum_{j=1}^{N_{\hat{\Gamma}}} n_{\xi,j} \mathsf{R}_j^T \mathsf{B}_j \mathsf{R}_j, \tag{3}$$

where $n_{\xi,j}$ is the ξ component of the outward pointing unit normal on facet j and $\mathsf{B}_j = diag\left(b_1^{(j)}, \ldots, b_{n_j}^{(j)}\right)$.

In order to construct the SBP derivative operator, an invertible square matrix that holds the Vandermonde matrix V as well as a square matrix that holds the matrix V_ξ are required [14]. If $n = N_{p,d}^*$, then both of these matrices are already square and the Vandermonde matrix is already invertible (since the columns of V are linearly independent). However, for $n > N_{p,d}^*$ we construct

$$\tilde{\mathsf{V}} = [\mathsf{V}\, \mathsf{W}],$$

where W is a matrix of size $n \times (n - N_{p,d}^*)$ with columns that are linearly independent to each other and to the columns of V. This ensures that the matrix $\tilde{\mathsf{V}}$ is invertible. For the matrix that holds V_ξ, we construct

$$\tilde{\mathsf{V}}_\xi = [\mathsf{V}_\xi\, \mathsf{W}_\xi],$$

where W_ξ has the same size as W but its entries are used to ensure S_ξ is skew symmetric. Condition 1 of Definition 1 can be recast as

$$\mathsf{D}\tilde{\mathsf{V}} = \tilde{\mathsf{V}}_\xi.$$

Now, by using conditions 2 and 3 of Definition 1 we find the following relation for S_ξ

$$\begin{aligned}
\mathsf{D}_\xi \tilde{\mathsf{V}} &= \tilde{\mathsf{V}}_\xi \\
\mathsf{H}^{-1}\mathsf{Q}_\xi \tilde{\mathsf{V}} &= \tilde{\mathsf{V}}_\xi \\
\left(\mathsf{S}_\xi + \frac{1}{2}\mathsf{E}_\xi\right)\tilde{\mathsf{V}} &= \mathsf{H}\tilde{\mathsf{V}}_\xi \qquad (4) \\
\mathsf{S}_\xi &= \mathsf{H}\tilde{\mathsf{V}}_\xi \left(\tilde{\mathsf{V}}\right)^{-1} - \frac{1}{2}\mathsf{E}_\xi \\
\mathsf{S}_\xi &= \mathsf{H}_\xi([\mathsf{V}_\xi\, \mathsf{W}_\xi])\left([\mathsf{V}\, \mathsf{W}]\right)^{-1} - \frac{1}{2}\mathsf{E}_\xi. \qquad (5)
\end{aligned}$$

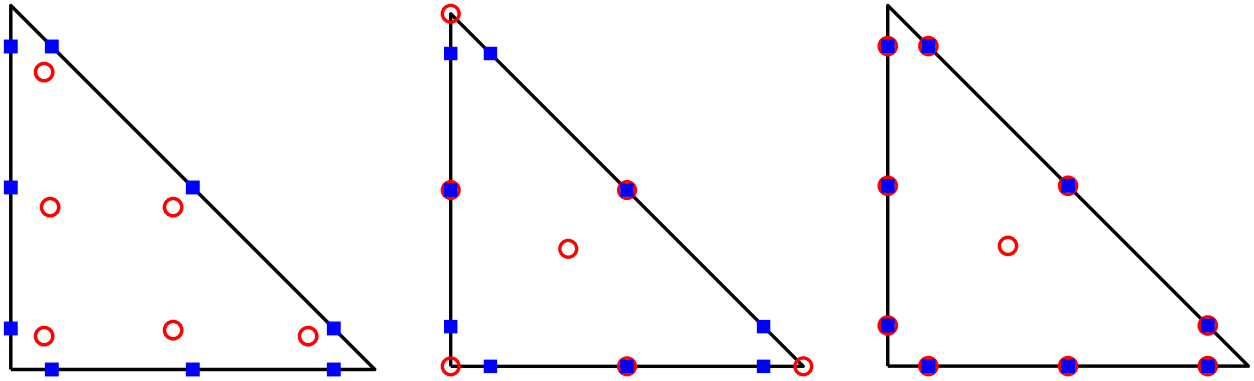

(a) Ω (6 ○ nodes) (b) Γ (7 ○ nodes) (c) diagonal-E (10 ○ nodes)

Fig. 1 $p = 2$ operators for three SBP families on triangles where ○ are the element nodes and ■ are the facet nodes.

The only requirement that remains to be shown is that S_ξ can be constructed to be skew symmetric using the undefined matrix W_ξ. This is demonstrated in [14]. The operators Q_ξ and D_ξ can then be constructed from S_ξ and E_ξ from the relations in Definition 1.

B. SBP families

There have been three general families of SBP operators that have been previously created on two and three dimensional simplex elments, the Ω, Γ and the diagonal-E families [13, 14, 30, 31]. The Ω family does not require any of its element nodes to be on its facets and as such, typically only has nodes that are within the element. The Ω family often has the minimum required number of nodes and has the cubature rule of the highest degree or with the lowest leading truncation error. The Γ family has nodes on the facets and only uses these element nodes on a given facet to interpolate/extrapolate the solution to the facet nodes of the same facet. Since the solution is interpolated/extrapolated from the volume nodes that are on the facets, only $N_{p,d-1}$ nodes are used for the interpolation/extrapolating instead of the $N_{p,d}$ required for the Ω operator. While the Γ operator typically has more nodes than the Ω operator, it has a lower interpolation/extrapolation cost. Finally, for the diagonal-E family, each of its facet nodes is collocated with one of its element nodes. This collocation of the nodes eliminates the need to interpolate/extrapolate the solution from the element nodes to the facet nodes since the solution is already known at the facet nodes. However, the diagonal-E family generally has the largest number of element nodes out of the three SBP families. Examples of the three SBP families are shown in Fig. 1.

III. Construction of optimized multidimensional summation-by-parts operators

The method presented in the previous section creates valid SBP operators, but they may not necessarily be optimal. When $n > N^*_{p,d}$, there are generally free parameters that can be used to optimize the SBP operator. This section shows how the construction of SBP operators can be modified such that the free parameters become available for optimization. While the methodology of the previous section is applicable to non-symmetrical nodal distributions, the optimization of SBP operators in this paper utilizes exclusively symmetrical nodal distributions. This has several advantages, such as being able to use the equations from [17] to derive cubature rules algebraically in order to have free parameters for the nodal locations and cubature weights to optimize the SBP operators.

A. Algebraic construction of symmetric cubature rules

In order to investigate the impact of the nodal locations and the cubature weights on the properties of the SBP operators it is beneficial to construct the cubature rules symbolically rather than numerically. Liu and Vinokur [17] derived equations to generate cubature rules for simplex elements with symmetrically located nodes. Examples of symmetric cubature rules in one dimension would be the Legendre-Gauss and Legendre-Gauss-Lobatto cubature rules. For the nodes to be symmetrically located in the simplex element they need to be part of a symmetry group. Table 1

Table 1 Primary symmetry groups for simplices.

	Description	Degrees of freedom (DOF)	Line		Triangle		Tetrahedron	
			n	$\frac{n}{\text{DOF}}$	n	$\frac{n}{\text{DOF}}$	n	$\frac{n}{\text{DOF}}$
s_{cent}	Centroid	1	1	1	1	1	1	1
$s_{\text{c-vert}}$	Vertex centered	2	2	1	3	1.5	4	2
$s_{\text{c-edge}}$	Edge centered	3			6	2	12	4
$s_{\text{c-mid-edge}}$	Mid-edge centered	2					6	3
$s_{\text{c-face}}$	Face centered	4					24	6

Table 2 Minimum number of required degrees of freedom to have a cubature rule of degree one to five on a simplex element with nodes in symmetry groups.

	Required number of DOF				
p_{cub}	1	2	3	4	5
Line	1	2	2	3	3
Triangle	1	2	3	4	5
Tetrahedron	1	2	3	5	6

shows the different symmetry groups that exist for one, two and three dimensional simplex elements.

All the nodes in a symmetry group have the same cubature weight and have at least one degree of freedom. The other degrees of freedom come from the nodal locations of the symmetry group. The symmetry groups with the smaller ratio of nodes to degrees of freedom are desirable in order to create cubature rules of the highest degree with the fewest nodes. However, Liu and Vinokur [17] demonstrated that just using the symmetry groups with the smallest ratio of nodes to degrees of freedom does not always satisfy all of the required equations in multiple dimensions. For example, a cubature rule of degree four or higher on a tetrahedron requires at least one $s_{\text{c-edge}}$ or $s_{\text{c-mid-edge}}$ (or possibly $s_{\text{c-face}}$, the authors in [17] did not consider this symmetry group and hence it may be applicable) symmetry group to be used. The number of degrees of freedom required to achieve a cubature rule of a given degree is shown in Table 2. Having the minimum required number of degrees of freedom does not guarantee that there is a cubature rule of the desired degree since SBP operators require the nodal locations to be real and the cubature weights to be both real and positive. Additionally, only SBP operators that have all of their nodes within the element are considered in this paper.

The Γ and diagonal-E operators require some of their element nodes to be on the facets. These nodes lie in one of the degenerate symmetry groups listed in Table 3. These symmetry groups have one fewer degree of freedom than their primary symmetry group counterpart listed in Table 1 since one degree of freedom is used to have the nodes on the facets. However, if the element nodes for a symmetry group are required to be collocated with the facet nodes, then this symmetry group only has one degree of freedom from its cubature weight. The three symmetry groups for a triangle and their degenerate groups that lie on the facets are plotted in Fig. 2. The shape of the reference triangle is not important for the nodal locations since a linear mapping can be used to transform the right triangle to a triangle of any size or shape. The nodes for the $s_{\text{c-vert}}$ symmetry group vary along the dotted symmetry lines that connect the vertices to the centroid of the opposing facets. Meanwhile, for the $s_{\text{c-edge}}$ symmetry group, there is one node in each of the six quadrants of the triangle as divided by the dotted symmetry lines. Examples of the symmetry groups for a tetrahedron are shown in Fig. 3. Only the nodes centered along one vertex, mid-edge or edge are plotted for clarity. The $s_{\text{c-face}}$ and s_{face} symmetry groups are not plotted but are similar to the $s_{\text{c-edge}}$ and s_{edge} symmetry groups for the triangle shown in Fig. 2b.

Combinations of these symmetry groups will be used to construct operators on tetrahedron element and cubature rules on triangular facets in the subsequent sections. One advantage of exclusively using nodes in symmetry groups is that the directional operators S, E, Q, and D only need to be constructed and optimized for one computational direction (e.g. ξ) and can then be transformed to the other directions (η and ζ). For this paper, a trirectangular tetrahedron (a tetrahedron that has three of its faces as right triangles) with vertices at (0,0,0), (1,0,0), (0,1,0) and (0,0,1) is used as the reference element to construct the cubature rules and SBP operators.

Table 3 Symmetry groups for simplices that have the nodes on the facets.

Sym groups on facets	Nodal locations	Primary sym group	Facet equiv. sym group	line	tri	tet
s_{vert}	On the vertices	$s_{\text{c-vert}}$	s_{vert}	✓	✓	✓
s_{edge}	On the edges	$s_{\text{c-edge}}$	$s_{\text{c-vert}}$(line) s_{edge}(tri)		✓	✓
$s_{\text{mid-edge}}$	On the mid-edges	$s_{\text{c-mid-edge}}$(tet) $s_{\text{c-vert}}$(tri)	$s_{\text{mid-edge}}$		✓	✓
$s_{\text{face-cent}}$	Centroid of the faces	$s_{\text{c-vert}}$	s_{cent}			✓
$s_{\text{c-face-vert}}$	Vertex centered on the faces	$s_{\text{c-edge}}$	$s_{\text{c-vert}}$			✓
s_{face}	On the faces	$s_{\text{c-face}}$	$s_{\text{c-edge}}$			✓

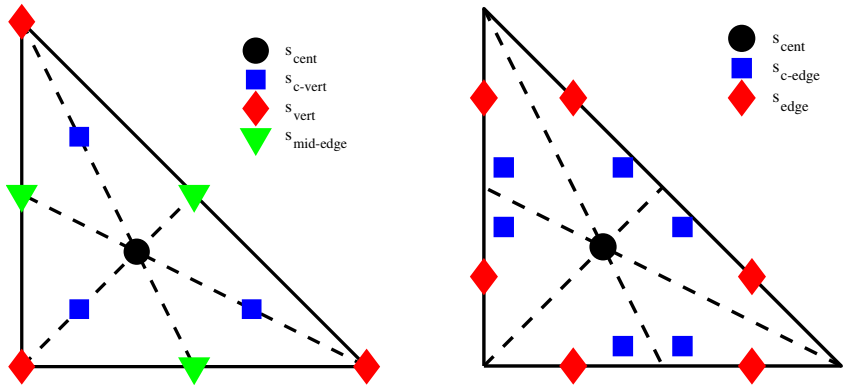

(a) Vertex centered **(b) Edge centered**

Fig. 2 Nodal symmetry groups for triangles.

B. Construction of SBP operators with free parameters

When $n > N^*_{p,d}$ the system of equations is underdetermined and could therefore be solved for free parameters. However, Eq. (2) uses the Moore-Penrose pseudoinverse to solve for R_j, which returns a unique solution with no free parameters. Taking the transpose of Eq. (1) gives

$$\underbrace{\mathsf{V}^T_{\hat{\Omega}}}_{\mathsf{A}} \underbrace{\mathsf{R}^T_j}_{\boldsymbol{x}} = \underbrace{\mathsf{V}^T_{\hat{\Gamma}_j}}_{\mathsf{b}}. \tag{6}$$

The matrices $\mathsf{V}_{\hat{\Omega}}$, R_j, and $\mathsf{V}_{\hat{\Gamma}_j}$ are of size $n \times N^*_{p,d}$, $n_j \times n$, and $n_j \times N^*_{p,d}$, respectively, where n_j is the number of nodes on facet j. A separate system of equations can be solved for each column of R^T_j independently. In this way, the equations are solved like a typical system of linear equations. Each column of R^T_j is used to interpolate/extrapolate the solution from the volume nodes to one facet node.

The operator E_ξ can be constructed using Eq. (3), which use the previously constructed R. In the construction of S_ξ in the previous section, the matrix W was selected with the only criterion that it ensures that $\tilde{\mathsf{V}}$ has independent columns. When $n > N^*_{p,d}$, there are an infinite number of matrices W that fit this criterion. In order to construct the matrices D_ξ and Q_ξ with all of the free parameters undefined, we begin with Eq. (4) but replace $\tilde{\mathsf{V}}$ and $\tilde{\mathsf{V}}_\xi$ with V and

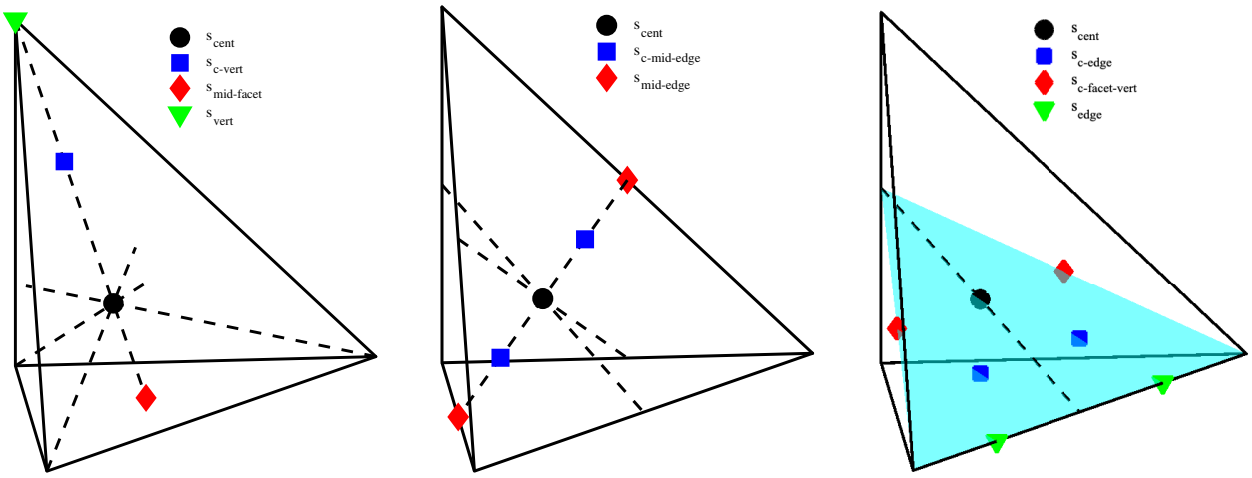

(a) Vertex centered **(b) Mid-edge centered** **(c) Edge centered**

Fig. 3 Nodal symmetry groups along one vertex, mid-edge or edge for tetrahedra.

V_ξ, respectively,

$$\begin{aligned}\left(\mathsf{S}_\xi + \frac{1}{2}\mathsf{E}_\xi\right)\mathsf{V} &= \mathsf{H}\mathsf{V}_\xi \\ \left(\mathsf{S}_\xi\mathsf{V}\right)^T &= \left(\mathsf{H}\mathsf{V}_\xi - \frac{1}{2}\mathsf{E}_\xi\mathsf{V}\right)^T \\ \underbrace{\mathsf{V}^T}_{A}\ \underbrace{\mathsf{S}_\xi}_{\boldsymbol{x}} &= \underbrace{\frac{1}{2}\mathsf{V}^T\mathsf{E}_\xi - \mathsf{V}_\xi^T\mathsf{H}}_{\boldsymbol{b}},\end{aligned} \tag{7}$$

where we used the symmetry of H and E_ξ as well as the skew-symmetric form of S_ξ to simplify the final result. The matrix S_ξ is skew symmetric and has $\frac{n(n-1)}{2}$ independent entries that are used to satisfy Eq. (7). There are a total of $n \times N^*_{p,d}$ linear equations in Eq. (7) that need to be solved to identify any free parameters. There are more equations than unknowns, but not all of the equations are linearly independent and thus the problem is not overdetermined [13].

IV. Objective functions and numerical test case

To investigate the optimization of the SBP operators, objective functions are evaluated and a numerical test case is run with SBP operators evaluated with a range of values for the free parameters. This process identifies whether there is a connection between optimizing the SBP operators for certain objective functions and minimizing the solution error for the test cases.

A. Objective functions

The element integration error is defined as

$$e_{\text{elem-int}} = \sqrt{\sum_{k=N^*_{p,d}+1}^{N^*_{p+1,d}} \left(\mathbf{1}^T\mathsf{H}\boldsymbol{p}_k - I_{\hat{\Omega},k}\right)^2}, \tag{8}$$

where $\mathbf{1}$ is a vector of ones of length n, $I_{\hat{\Omega},k}$ is the exact integration of the k-th polynomial over $\hat{\Omega}$, and $e_{\text{elem-int}}$ is the L^2 norm of the error of the numerical integration over $\hat{\Omega}$. This objective function is used when there are free parameters in the cubature rule, either from the nodal locations or the cubature weights.

The interpolation/extrapolation error is calculated as

$$e_{\text{int/ext}} = \sqrt{\sum_{k=N^*_{p,d}+1}^{N^*_{p+1,d}} (\mathsf{R}_1 \boldsymbol{p}_k - \boldsymbol{p}_{f,k})^T \mathsf{B} (\mathsf{R}_1 \boldsymbol{p}_k - \boldsymbol{p}_{f,k})}, \tag{9}$$

where $\boldsymbol{p}_{f,k}$ is the evaluation of the k-th basis function to the facet cubature nodes on facet one.

The facet integration error is calculated by considering the integration error over facet one

$$e_{\text{facet-int}} = \sqrt{\sum_{k=N^*_{p,d-1}+1}^{N^*_{p+1,d-1}} \left(\mathbf{1}^T \mathsf{B}_1 \mathsf{R}_1 \boldsymbol{p}_k - I_{\hat{\Gamma}_1,k} \right)^2}, \tag{10}$$

where $\mathbf{1}$ is of length n_j, $I_{\hat{\Gamma}_1,k}$ is the exact integration of the k-th polynomial over $\hat{\Gamma}_1$, and $e_{\text{facet-int}}$ is the L^2 norm of the error of the numerical integration over $\hat{\Gamma}_1$. This objective function is used when there are free parameters in the interpolation/extrapolation operator R_1.

When there are free parameters in the skew-symmetric matrix S_ξ, the objective function that is used is the leading truncation term, which is calculated as

$$e_{\text{derivative}} = \sqrt{\sum_{k=N^*_{p,d}+1}^{N^*_{p+1,d}} (\mathsf{D}_\xi \boldsymbol{p}_k - \boldsymbol{p}'_k)^T \mathsf{H} (\mathsf{D}_\xi \boldsymbol{p}_k - \boldsymbol{p}'_k)}. \tag{11}$$

The Frobenius norm of a matrix is defined as

$$||\mathsf{A}||_F = \sqrt{\text{Tr}(\mathsf{A}^H \mathsf{A})} = \sqrt{\sum_{i=1}^{m_1} \sum_{j=1}^{m_2} |a_{i,j}|^2}, \tag{12}$$

where A is a m_1 by m_2 matrix, A^H is the conjugate transpose of A, and Tr takes the trace of a matrix. Since all the SBP matrices that are used have exclusively real entries, the ordinary transpose can be used in place of the conjugate transpose and the absolute values are not required since each entry in A is squared. The Frobenius norm bounds the spectral radius as

$$\rho(\mathsf{A}) \leq ||\mathsf{A}||_F, \tag{13}$$

where $\rho(\mathsf{A})$ is the spectral radius of A [32]. We define A as

$$\mathsf{A} = \mathsf{D}_\xi + \mathsf{R}_1^T \mathsf{B}_1 \mathsf{R}_1, \tag{14}$$

which takes into account the derivative operator and an approximation to an upwind SAT.

The solution error for the test case is calculated using the broken H norm $||\boldsymbol{u}_n - \boldsymbol{u}_e||_{\mathsf{H}_g}$, where $\boldsymbol{u}_n$ and $\boldsymbol{u}_e$ are the numerical and exact solutions, respectively. The solution errors that are presented for one operator with one or two varying free parameters are normalized using the minimum solution error.

B. Test case

The test case that is solved to investigate the properties of the SBP operators is the three-dimensional linear advection equation

$$\frac{\partial \mathcal{U}}{\partial t} + \frac{\partial a_x \mathcal{U}}{\partial x} + \frac{\partial a_y \mathcal{U}}{\partial y} + \frac{\partial a_z \mathcal{U}}{\partial z} = 0, \tag{15}$$

where a_x, a_y and a_z are the constant velocities in the x, y and z directions, respectively. The domain $\Omega \in \mathbb{R}^3$ is discretized into K non-overlapping elements $\bar{\Omega} = \cup_{k=1}^K \Omega_k$ and $\Omega_i \cap \Omega_j = \emptyset, \forall i \neq j$. For each element Ω_k, Eq. (15) is mapped from physical to computational coordinates:

$$\frac{\partial \mathcal{J}\mathcal{U}}{\partial t} + \frac{\partial a_\xi \mathcal{U}}{\partial \xi} + \frac{\partial a_\eta \mathcal{U}}{\partial \eta} + \frac{\partial a_\zeta \mathcal{U}}{\partial \zeta} = 0, \tag{16}$$

where $\mathcal{J}$ is the metric Jacobian, while a_ξ, a_η and a_ζ are the velocities in the curvilinear coordinates. The mesh is curved using the following transformation:

$$
\begin{aligned}
x' &\leftarrow x + \frac{1}{20}\cos\big(\pi(x-0.5)\big)\cos\big(\pi(y-0.5)\big)\cos\big(\pi(z-0.5)\big), \\
y' &\leftarrow y + \frac{1}{20}\cos\big(\pi(x-0.5)\big)\cos\big(\pi(y-0.5)\big)\cos\big(\pi(z-0.5)\big), \\
z' &\leftarrow y + \frac{1}{20}\cos\big(\pi(x-0.5)\big)\cos\big(\pi(y-0.5)\big)\cos\big(\pi(z-0.5)\big).
\end{aligned}
$$

Upwind SATs are applied as described in [14]. The domain is discretized into a structured hexahedral mesh on the domain $[0,1]\times[0,1]\times[0,1]$ and each hexahedron is split into six tetrahedra. Periodic boundary conditions are applied and the initial solution is set to $u_0 = \exp\left(-\frac{x^2+y^2+z^2}{2\sigma^2}\right)$. The solution is marched through time using a fourth-order Runge-Kutta (RK4) method with time steps calculated as $\Delta t = \frac{\text{CFL}\,\min(\Delta x,\Delta y,\Delta z)}{\max(a_x,a_y,a_z)}$, where CFL is the Courant-Friedrichs-Lewy number, which is set to 0.05, unless indicated otherwise, Δx, Δy and Δz are taken as the average size of one hexahedron element in that respective Cartesian direction, and the wave speeds a_x, a_y and a_z are all set to $1/2$. The CFL number was selected to be small enough such that the primary source of the error comes from the spatial discretization instead of the temporal discretization, with the exception of operators that have their nodes nearly collocated. A constant CFL number is used for all of the operators in order to have an unbiased comparison of the different operators.

When free parameters in an operator are being investigated there are a total of $8\times8\times8 = 512$ hexahedra and thus 3072 tetraheral elements. When the efficiency of different operators are compared a set of finer meshes is used. The coarsest mesh has $6\times6\times6 = 216$ hexahedra for a total of 1296 tetrahedral elements. Each subsequent mesh has three tetrahedral elements added in each direction. As such, the second mesh has 4374 ($9^3\times6$) tetrahedral elements.

V. Results for Ω operators

The minimum number of nodes required for a $p = 1$ operator on a tetrahedron is $N^*_{1,3} = 4$. Table 1 indicates that $s_{\text{c-vert}}$ has four nodes and two degrees of freedom for the cubature rule. A $p = 1$ operator only requires a cubature rule of degree $2p-1 = 1$. After satisfying the requirement to have a cubature rule of degree one, the nodal locations remain a free parameter. The nodal locations, cubature weights, interpolation/extrapolation operator and the derivative operator are given by

$$
S_{\hat{\Omega}} = \begin{bmatrix} \frac{1-t_1}{4} & \frac{1-t_1}{4} & \frac{1-t_1}{4} \\ \frac{3t_1+1}{4} & \frac{1-t_1}{4} & \frac{1-t_1}{4} \\ \frac{1-t_1}{4} & \frac{3t_1+1}{4} & \frac{1-t_1}{4} \\ \frac{1-t_1}{4} & \frac{1-t_1}{4} & \frac{3t_1+1}{4} \end{bmatrix}, \qquad
\mathsf{R}_1 = \begin{bmatrix} \frac{t_1-1}{4t_1} & \frac{3t_1+5}{12t_1} & \frac{3t_1-1}{12t_1} & \frac{3t_1-1}{12t_1} \\ \frac{t_1-1}{4t_1} & \frac{3t_1-1}{12t_1} & \frac{3t_1+5}{12t_1} & \frac{3t_1-1}{12t_1} \\ \frac{t_1-1}{4t_1} & \frac{3t_1-1}{12t_1} & \frac{3t_1-1}{12t_1} & \frac{3t_1+5}{12t_1} \end{bmatrix},
$$

$$
\mathsf{H} = \begin{bmatrix} \frac{1}{24} & 0 & 0 & 0 \\ 0 & \frac{1}{24} & 0 & 0 \\ 0 & 0 & \frac{1}{24} & 0 \\ 0 & 0 & 0 & \frac{1}{24} \end{bmatrix}, \qquad
\mathsf{D}_\xi = \begin{bmatrix} -\frac{1}{t_1} & \frac{1}{t_1} & 0 & 0 \\ -\frac{1}{t_1} & \frac{1}{t_1} & 0 & 0 \\ -\frac{1}{t_1} & \frac{1}{t_1} & 0 & 0 \\ -\frac{1}{t_1} & \frac{1}{t_1} & 0 & 0 \end{bmatrix}, \tag{17}
$$

where $-1/3 \le t_1 \le 1$ ensures that the nodes are on or within the reference element.

Fig. 4a shows how the free parameter varies as the nodes are moved from the vertices to the centroid of the opposing facet. Meanwhile, Fig. 4b shows the solution error and select objective functions. The global minimum of the solution error coincides with the minimum of the element integration error, which has an error of zero, indicating a cubature rule of degree two. There is one more nodal location that provides a cubature rule of degree two but it requires the nodes to lie outside of the reference element, but this case is not considered in this paper. There is a gap in the solution error in Fig. 4b when the free parameter is near zero since the nodes become collocated at this value. As the nodes get closer together, the evaluation of $||\mathsf{A}||_F$ increases rapidly and tends to infinity. However, the location where the nodes are collocated is also where $e_{\text{derivative}}$ is minimized. The objective $e_{\text{derivative}}$ is minimized as the nodes get closer together

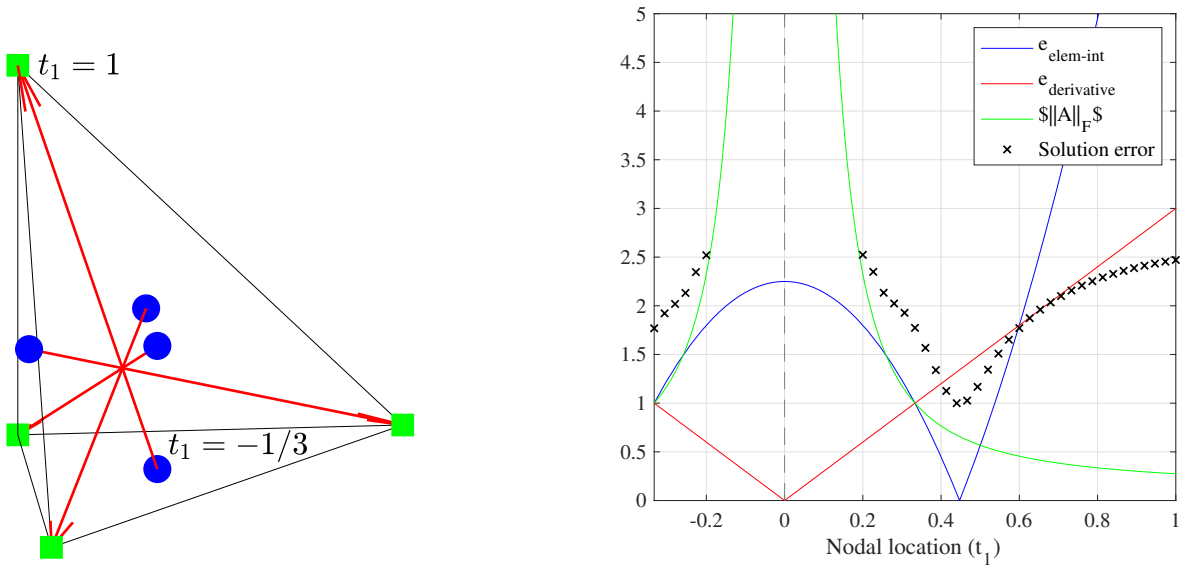

(a) Nodal locations **(b) Normalized solution error and objective functions**

Fig. 4 Nodal locations and solutions error for $p = 1$ tetrahedron operator with one $s_{c\text{-vert}}$.

since a finite-difference scheme is more accurate at calculating derivatives as the nodal spacing is reduced. It is clear from this example that $e_{\text{elem-int}}$ is a good objective to optimize the free parameters for the nodal locations in order to minimize the solution error. However, it is important that $||\mathsf{A}||_F$ remain small since it bounds the spectral radius. The objective $e_{\text{derivative}}$ is not a good indicator of how to minimize the solution error for free parameters in the cubature rule.

For the next operator, the symmetry group $s_{c\text{-vert}}$ is kept and the s_{cent} node is added for a total of five nodes. After satisfying the equation from Liu and Vinokur [17] to have a cubature rule of degree one, two free parameters in the cubature rule remain. There is also one free parameter in R_1 for the contribution of the s_{cent} node to the interpolation/extrapolation of the solution from the volume nodes to the facet nodes. The $S_{\hat{\Omega}}$, H, R_1 and D_ξ matrices are given by

$$S_{\hat{\Omega}} = \begin{bmatrix} \frac{1}{4} & \frac{1}{4} & \frac{1}{4} \\ \frac{1-t_1}{4} & \frac{1-t_1}{4} & \frac{1-t_1}{4} \\ \frac{3t_1+1}{4} & \frac{1-t_1}{4} & \frac{1-t_1}{4} \\ \frac{1-t_1}{4} & \frac{3t_1+1}{4} & \frac{1-t_1}{4} \\ \frac{1-t_1}{4} & \frac{1-t_1}{4} & \frac{3t_1+1}{4} \end{bmatrix}, \qquad \mathsf{R}_1 = \begin{bmatrix} r_1 & \frac{t_1-1}{4t_1} - \frac{r_1}{4} & \frac{3t_1+5}{12t_1} - \frac{r_1}{4} & \frac{3t_1-1}{12t_1} - \frac{r_1}{4} & \frac{3t_1-1}{12t_1} - \frac{r_1}{4} \\ r_1 & \frac{t_1-1}{4t_1} - \frac{r_1}{4} & \frac{3t_1-1}{12t_1} - \frac{r_1}{4} & \frac{3t_1+5}{12t_1} - \frac{r_1}{4} & \frac{3t_1-1}{12t_1} - \frac{r_1}{4} \\ r_1 & \frac{t_1-1}{4t_1} - \frac{r_1}{4} & \frac{3t_1-1}{12t_1} - \frac{r_1}{4} & \frac{3t_1-1}{12t_1} - \frac{r_1}{4} & \frac{3t_1+5}{12t_1} - \frac{r_1}{4} \end{bmatrix},$$

$$\mathsf{H} = \begin{bmatrix} \frac{1-4w_1}{6} & 0 & 0 & 0 & 0 \\ 0 & \frac{w_1}{6} & 0 & 0 & 0 \\ 0 & 0 & \frac{w_1}{6} & 0 & 0 \\ 0 & 0 & 0 & \frac{w_1}{6} & 0 \\ 0 & 0 & 0 & 0 & \frac{w_1}{6} \end{bmatrix}, \quad \mathsf{D}_\xi = \begin{bmatrix} 0 & -\frac{1}{t_1} & \frac{1}{t_1} & 0 & 0 \\ -\frac{4w_1+r_1-1}{w_1 t_1} & \frac{r_1-1}{4w_1 t_1} & \frac{8w_1+r_1-1}{4w_1 t_1} & \frac{4w_1+r_1-1}{4w_1 t_1} & \frac{4w_1+r_1-1}{4w_1 t_1} \\ \frac{4w_1+r_1-1}{w_1 t_1} & -\frac{8w_1+r_1-1}{4w_1 t_1} & -\frac{r_1-1}{4w_1 t_1} & -\frac{4w_1+r_1-1}{4w_1 t_1} & -\frac{4w_1+r_1-1}{4w_1 t_1} \\ 0 & -\frac{1}{t_1} & \frac{1}{t_1} & 0 & 0 \\ 0 & -\frac{1}{t_1} & \frac{1}{t_1} & 0 & 0 \end{bmatrix}. \tag{18}$$

Each column of R_1 represents the contribution of one element node to each of the facet nodes, while each row in R_1 is the contribution of all of the element nodes to one facet node. The first column of R_1 is the contribution of the s_{cent} node to each of the facet nodes. Since the facet nodes are symmetrically located on the facet (they are in the $s_{c\text{-vert}}$ group), they each have the same contribution from the element's s_{cent} node, r_1. Therefore, if $r_1 = 0$, the s_{cent} node does not contribute to the interpolation/extrapolation of the solution to the facet cubature nodes. To have all the weights be positive in H, it is required that $0 < w_1 < 1/4$. When $w_1 = 0$, the weight is zero on all of the $s_{c\text{-vert}}$ nodes, while having $w_1 = 1/4$ makes the weight on the s_{cent} node be zero. As such, the operator in (17) is recovered when $r_1 = 0$ and $w_1 = 1/4$ since t_1 is the same free parameter for both operators.

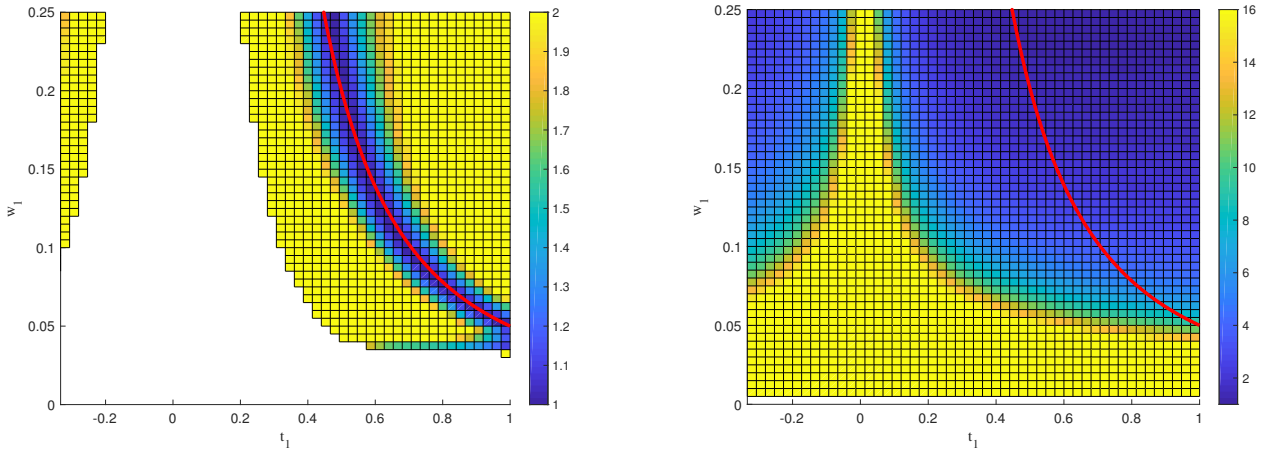

(a) Normalized solution error **(b) Normalized Frobenius norm of A**

Fig. 5 $p = 1$ **tetrahedron operator with one** s_{cent} **and** $s_{c\text{-}vert}$ **symmetry groups with no contribution from the** s_{cent} **node to the interpolation/extrapolation of the solution to the facet cubature nodes and where the red line indicates** $p_{cub} = 2$**.**

Fig. 5a plots the normalized numerical error as the two free parameters from the cubature rule are varied and r_1 is set to zero. Just like the previous test case in Fig. 4b, the solution error is minimized when the cubature rule is of degree two, as indicated by the red line in Fig. 5. Fig. 5b shows the Frobenius norm of A. The locations where the Frobenius norm is large coincide with the locations that the operators are not stable using RK4 and CFL = 0.05, shown as white space in Fig. 5a.

When a cubature rule of degree two is enforced, this leads to the following relation between the cubature weight, w_1, and the free parameter for the nodal location, t_1:

$$w_1 = \frac{1}{20t_1^2}, \tag{19}$$

where $\sqrt{1/5} < t_1 \leq 1$ ensures all the weights are positive and that the nodes are within the element. When $t_1 < \sqrt{1/5}$, the weight on the s_{cent} node is negative and when $t_1 > 1$, the $s_{c\text{-}vert}$ nodes pass the vertices and are outside of the reference element. The new operator now only has t_1 and r_1 as free parameters, which allows r_1 to be varied on a two-dimensional surface plot. Fig. 6a shows that for all the nodal locations considered, the solution error is around 40% higher than the minimum solution error when the contribution from the s_{cent} node is between zero and one. Since r_1 is a free parameter in R_1, which is used to interpolate/extrapolate the solution from the volume nodes to the facet nodes and then integrate the solution over the facet, it is logical to consider optimizing r_1 to minimize either $e_{int/ext}$ or $e_{facet\text{-}int}$. However, Fig. 6c and Fig. 6d show that the minima of these errors do not coincide with the minimum of the solution error. Fig. 6b shows that the increase in solution error when r_1 is between zero and one coincides with an increase in the dissipation of the kinetic energy. A difference in solution error of only 40% is small compared to the 250% difference between the minimum and maximum solution error in Fig. 4. However, this example indicates that when there are free parameters in R_1, they can be used to adjust the level of dissipation, which may be helpful for problems where additional dissipation is required.

Since the derivative operator D_ξ is constructed from E_ξ, which is itself constructed from R_1, the free parameters in R_1 are also present in D_ξ, as shown in (18). Fig. 6e and 6f show the Frobenius norm for D_ξ and A, respectively. It is evident that the stable region for the scheme, shown by coloured cells in Fig. 6a, coincides more closely with the minimum of the Frobenius norm of A. Considering the values along the left edge of the plots ($t_1 = \sqrt{1/5} \approx 0.45$), the left-most column of blocks in Fig. 6a is missing, indicating that these operators are not stable with the the selected time marching method. For this same column of blocks, the Frobenius norm is high for A at all values of r_1, while the Frobenius norm of D_ξ is low for $-1 < r_1 < 1.5$. The scheme is unstable when $t_1 = \sqrt{1/5}$, since $w_1 = 0.25$ and the weight on the s_{cent} node is zero. To understand the difference in the Frobenius norm of A and D_ξ, the inverse of H must be considered. Since H is diagonal, it is in the form $\mathsf{H} = \mathrm{diag}(h_1, h_2, \ldots, h_n)$ and thus $\mathsf{H}^{-1} = \mathrm{diag}(1/h_1, 1/h_2, \ldots, 1/h_n)$. Therefore, if one of the cubature weights goes to zero, at least one of the entries in H^{-1} tends to infinity. Since A includes H^{-1}, very small cubature weights therefore have a large impact on the Frobenius norm of A, while they do not impact

Table 4 Properties of symmetry groups on a tetrahedron with nodes on the facets.

Element symmetry groups	n	n_f	n/n_f	DOF	n / DOF
s_{vert}	4	3	4/3	1	4
s_{edge}	12	6	2	2	6
$s_{\text{mid-edge}}$	6	3	2	1	6
$s_{\text{face-cent}}$	4	1	4	1	4
$s_{\text{c-face-vert}}$	12	3	4	2	6
s_{face}	24	6	4	3	8

Table 5 Symmetry groups for $p = 1$ Γ family.

Element sym groups with facet nodes	Additional element sym groups	n	p_{cub}
s_{vert}		4	1
s_{vert}	s_{cent}	5	2
s_{vert}	$s_{\text{c-vert}}$	8	3

the Frobenius norm of D_ξ. Therefore, the Frobenius norm of A provides a better indication of whether a scheme will have a large spectral radius and hence will require a very small time step with an explicit time-marching method.

VI. Results for Γ operators

To minimize the number of nodes for Γ operators it is beneficial to use symmetry groups that have nodes on the facets with the lowest ratio of volume to facet nodes (n/n_f) and also the lowest ratio of volume nodes to degrees of freedom for the cubature rule (n/DOF). Table 4 shows that the most desirable symmetry group to use is the s_{vert} group since it has the lowest ratio of both n/n_f and n/DOF. The $p = 1$ and $p = 2$ Γ operators respectively use the $p = 1$ and $p = 2$ element cubature rule from the Ω triangular element operators from [14] as their facet cubature rule of degree $2p$.

A. $p = 1$ Γ operators

For a $p = 1$ Γ operator on a tetrahedron, a minimum of $N^*_{1,3} = 4$ volume nodes and $N^*_{1,2} = 3$ facet nodes are required. Table 4 indicates that s_{vert} provides the minimum required number of both volume and facet nodes for a $p = 1$ Γ operator. Previous results indicated that increasing the cubature rule from $2p - 1$ to $2p$ is beneficial and thus, operators with additional symmetry groups and cubature rules of higher degrees are also generated. The symmetry groups from Table 1 with the lowest n/DOF ratio are selected, which provide the minimum degrees of freedom, as indicated by Table 2, for cubature rules with $p_{\text{cub}} = 1, 2$ and 3. Table 5 shows the generated operators, and Fig. 7a shows the results of these operators. The first operator in Table 5 was previously constructed in [13]. Fig. 7a shows that, once again, increasing p_{cub} from $2p - 1 = 1$ to $2p = 2$ provides for a more efficient operator. As for the operator with $p_{\text{cub}} = 2p + 1 = 3$, it was more computationally expensive for each of the meshes than the operator with $p_{\text{cub}} = 2$, which is expected since it has more nodes, but it also has a slightly higher solution error for each mesh. This result suggests that there is no benefit to increasing the degree of the cubature rule beyond $2p$.

B. $p = 2$ Γ operators

For a $p = 2$ Γ operator, there needs to be at least $N^*_{2,2} = 6$ nodes on each facet. Table 4 shows that the s_{vert}, $s_{\text{mid-edge}}$ and $s_{\text{c-face-vert}}$ symmetry groups all have three nodes, and thus any combination of two of these three symmetry groups can be used to have six nodes on each of the facets. Both the s_{edge} and s_{face} symmetry groups create a set of unisolvent nodes on the facets that cannot be used to interpolate the solution from the volume nodes to the facet nodes, since the Vandermonde matrix evaluated at the element nodes on each of the facets does not have linearly independent columns (as required to construct R_1). The generated operators use a combination of s_{vert}, $s_{\text{mid-edge}}$ and $s_{\text{c-face-vert}}$ symmetry

Table 6 Symmetry groups for $p = 2$ Γ family.

Element sym groups with facet nodes	Additional element sym groups	n	p_{cub}
$s_{\text{vert}} + s_{\text{mid-edge}}$	s_{cent}	11	3
	$2\, s_{\text{c-vert}}$	18	5
	$s_{\text{c-edge}}$	22	4
$s_{\text{c-face-vert}} + s_{\text{vert}}$	$s_{\text{c-vert}}$	20	4
	$s_{\text{cent}} + s_{\text{c-vert}}$	21	5
$s_{\text{c-face-vert}} + s_{\text{mid-edge}}$	$s_{\text{c-vert}}$	22	4

Table 7 Symmetry groups for $p = 1$ diagonal-E family.

Element sym groups with facet nodes	Additional element sym groups	n	p_{cub}
$s_{\text{c-edge}}$		6	1
	s_{cent}	7	2
	$s_{\text{c-vert}}$	10	3
$s_{\text{mid-edge}}$		12	1
	s_{cent}	13	2

groups, as shown in Table 6. The first operator in this table matches the $p = 2$ operator in [13].

For the numerical tests, the CFL number is set to 0.01 instead of 0.05, since only the first and fourth operators in Table 6 are stable at the larger CFL number. Fig. 7b shows that the operators with $p_{\text{cub}} = 2p = 4$ are more efficient that the operator with $p_{\text{cub}} = 2p - 1 = 3$ and have similar efficiency to the operators with $p_{\text{cub}} = 2p + 1 = 5$. All of the operators with $p_{\text{cub}} = 4, 5$ have similar efficiency, but the fourth operator is slightly more efficient for each subsequent finer mesh. The fourth operator also has the advantage of being stable at the larger CFL number of 0.05.

VII. Results for diagonal-E operators

For the diagonal-E operators, the symmetry groups for the element nodes must be selected such that each facet node is collocated with an element node. Therefore, the construction of diagonal-E operators begins with the selection of symmetry groups for a facet cubature rule with $p_{\text{cub}} = 2p$. Operators with $p = 1$ are considered first, followed by $p = 2$ operators.

A. $p = 1$ diagonal-E operators

Table 2 indicates that for a triangle, a cubature rule of degree two requires at least two degrees of freedom. Table 1 shows that for a triangle, the symmetry group $s_{\text{c-vert}}$ provides the necessary two degrees of freedom. When the equations from Liu and Vinokur [17] for a cubature rule of degree two with one $s_{\text{c-vert}}$ symmetry group are solved, there are two solutions that are shown in Fig. 8. Table 3 indicates that the first cubature rule, shown in Fig. 8a, requires the element symmetry group $s_{\text{c-edge}}$, which has 12 nodes. Meanwhile, the second cubature rule, shown in Fig. 8b, requires the element symmetry group $s_{\text{mid-edge}}$, which has only 6 nodes. Table 7 shows the symmetry groups used to create $p = 1$ diagonal-E operators with the two facet cubature rules in Fig. 8. The $p = 1$ diagonal-E operator from [31] has 13 nodes and matches the cubature rule for the $p_{\text{cub}} = 2$ operator with the $s_{\text{c-vert}}$ facet symmetry group derived independently in this paper.

The results for the test case for $p = 1$ diagonal-E operators are shown in Fig. 9a where, once more, the operators with $p_{\text{cub}} = 2p = 2$ have a significantly lower solution error compared to the operators with $p_{\text{cub}} = 2p - 1 = 1$. The operator with $p_{\text{cub}} = 3$ has a similar efficiency to both of the operators with $p_{\text{cub}} = 2$. The use of the $s_{\text{mid-edge}}$ facet symmetry group provides a more efficient diagonal-E operator when $p_{\text{cub}} = 1$, but a slightly less efficient operator when

Table 8 Possible combinations of symmetry groups for a facet cubature rule of degree four on a tetrahedral element.

ID	Element sym groups	Facet (triangle) sym groups	n	No. sym groups	Valid SBP cub rule
1	$s_{\text{face-cent}} + s_{\text{vert}} + s_{\text{c-face-vert}}$	$s_{\text{cent}} + s_{\text{vert}} + s_{\text{c-vert}}$	20	3	✗
2	$s_{\text{face-cent}} + s_{\text{vert}} + s_{\text{edge}}$	$s_{\text{cent}} + s_{\text{vert}} + s_{\text{c-vert}}$	20	3	✗
3	$s_{\text{face-cent}} + s_{\text{mid-edge}} + s_{\text{c-face-vert}}$	$s_{\text{cent}} + s_{\text{mid-edge}} + s_{\text{c-vert}}$	22	3	✓
4	$s_{\text{face-cent}} + s_{\text{mid-edge}} + s_{\text{edge}}$	$s_{\text{cent}} + s_{\text{mid-edge}} + s_{\text{edge}}$	22	3	✗
5	$s_{\text{vert}} + s_{\text{mid-edge}} + s_{\text{c-face-vert}}$	$s_{\text{vert}} + s_{\text{mid-edge}} + s_{\text{c-vert}}$	22	3	✓
6	$s_{\text{vert}} + s_{\text{mid-edge}} + s_{\text{edge}}$	$s_{\text{vert}} + s_{\text{mid-edge}} + s_{\text{edge}}$	22	3	✗
7	$2\, s_{\text{c-face-vert}}$	$2\, s_{\text{c-vert}}$	24	2	✓
8	$s_{\text{c-face-vert}} + s_{\text{edge}}$	$s_{\text{c-vert}} + s_{\text{edge}}$	24	2	✓
9	$2\, s_{\text{edge}}$	$2\, s_{\text{edge}}$	24	2	✗

Table 9 Symmetry groups for $p = 2$ diagonal-E family with $p_{\text{cub}} = 3, 4$.

Facet cub rule ID	Element sym groups with facet nodes	Additional element sym groups	n	p_{cub}
3	$s_{\text{face-cent}} + s_{\text{mid-edge}} + s_{\text{c-face-vert}}$	s_{cent}	23	3
		$s_{\text{c-vert}}$	26	4
7	$2\, s_{\text{c-face-vert}}$	s_{cent}	25	3
		$s_{\text{c-edge}}$	36	4
8	$s_{\text{c-face-vert}} + s_{\text{edge}}$	s_{cent}	25	3

$p_{\text{cub}} = 2$. While the operator with the $s_{\text{mid-edge}}$ facet symmetry group and $p_{\text{cub}} = 2$ has a slightly higher solution error, it is possible it would be more efficient than its counterpart with the $s_{\text{c-vert}}$ facet symmetry group and $p_{\text{cub}} = 2$ for a different test case, particularly one with discontinuities in the solution where smaller elements are beneficial.

B. $p = 2$ diagonal-E operators

The construction of $p = 2$ diagonal-E operators also begins by constructing facet cubature rules. Table 2 shows that four degrees of freedom are required to have a cubature rule of degree $2p = 4$ on the triangular facets. Combinations of the facet symmetry groups with a total of four degrees of freedom are selected. Table 8 shows the different combinations of symmetry groups used and whether a valid SBP cubature rule was found for the facet.

The facet cubature rules from Table 8, which are shown in Fig. 10, are used to create cubature rules on a tetrahedron with $p_{\text{cub}} = 2p - 1 = 3$ and $p_{\text{cub}} = 2p = 4$. Element symmetry groups with the nodes in the element are also needed to provide additional degrees of freedom such that a valid SBP cubature rule can be found. Table 9 shows the symmetry groups used for all the $p = 2$ operators. Only an element cubature rule of degree 3 was found for facet cubature rule 7, while no valid cubature rule for the tetrahedron could be found with facet cubature rule 8. All the combinations of additional element symmetry groups providing a sufficient number of degrees of freedom were tested up to a maximum of 36 nodes in an attempt to find cubature rules with $p_{\text{cub}} = 3, 4$. The cubature rule for the $p = 2$ diagonal-E operator from [31] has 36 nodes and matches the cubature rule of the $p_{\text{cub}} = 4$ with the seventh facet cubature rule from Table 8, which was derived independently. The results for these $p = 2$ diagonal-E operators for the numerical test case are shown in Fig. 9b. The results indicate that the two operators with $p_{\text{cub}} = 4$ are both more efficient that the operators with only $p_{\text{cub}} = 3$. Additionally, the $p_{\text{cub}} = 4$ operator with the third facet cubature rule from Table 8, is more efficient than the $p_{\text{cub}} = 4$ operator with the fifth facet cubature rule from Table 8, since it has 10 fewer nodes and yet still has a similar solution error for each mesh that was used.

VIII. Conclusion and future work

A systematic method of constructing SBP operators of the Ω, Γ and diagonal-E families using nodal symmetry groups was presented such that free parameters could be used to minimize desired objective functions. The results from this paper showed that there is a significant benefit to increasing the degree of the cubature rule from $2p-1$ to $2p$. Even with the additional computational cost associated with the extra nodes, the operators with $p_{\text{cub}} = 2p$ significantly reduced the solution error and are more efficient. However, there was no observed benefit of increasing the degree of the cubature rule from $2p$ to $2p+1$.

The Frobenius norm of A was shown to be a superior indicator of the spectral radius of the global operator than the Frobenius norm of D_ξ. It was also determined that free parameters in R_1 have a substantial impact on both the amount of dissipation and on the spectral radius. New and more efficient $p = 1$ and $p = 2$ operators for the Γ family were constructed compared to the operators from [13]. A new $p = 1$ diagonal-E operator with $p_{\text{cub}} = 2$ was constructed with nearly the same efficiency as the one from [31] but with 7 nodes instead of 13. Finally, a more efficient $p = 2$ diagonal-E operator with $p_{\text{cub}} = 4$ was constructed with 10 fewer nodes than the one from [31]. These operators are available upon request by emailing either of the authors.

Acknowledgments

The authors are thankful for the financial support granted by the University of Toronto, the Natural Sciences and Engineering Research Council of Canada and the Government of Ontario as well as the insight and support from Dr. Masayuki Yano.

References

[1] Gagnon, H., and Zingg, D. W., "Aerodynamic Optimization Trade Study of a Box-Wing Aircraft Configuration," *Journal of Aircraft*, Vol. 53, No. 4, 2016, pp. 971–981. doi:10.2514/6.2015-0695.

[2] Reist, T. A., and Zingg, D. W., "High-Fidelity Aerodynamic Shape Optimization of a Lifting-Fuselage Concept for Regional Aircraft," *Journal of Aircraft*, Vol. 54, No. 3, 2017, pp. 1085–1097. doi:10.2514/1.C033798.

[3] Del Rey Fernández, D. C., Hicken, J. E., and Zingg, D. W., "Review of Summation-by-Parts Operators with Simultaneous Approximation Terms for the Numerical Solution of Partial Differential Equations," *Computers & Fluids*, Vol. 95, 2014, pp. 171–196.

[4] Crean, J., Hicken, J. E., Del Rey Fernández, D. C., Zingg, D. W., and Carpenter, M. H., "Entropy-Stable Summation-by-Parts Discretization of the Euler Equations on General Curved Elements," *Journal of Computational Physics*, Vol. 356, 2018, pp. 410–438. doi:10.1016/j.jcp.2017.12.015.

[5] Svärd, M., "On Coordinate Transformations for Summation-by-Parts Operators," *Journal of Scientific Computing*, Vol. 20, No. 1, 2004, pp. 29–42.

[6] Kreiss, H.-O., and Oliger, J., "Comparison of Accurate Methods for the Integration of Hyperbolic Equations," *Tellus*, Vol. 24, No. 3, 1972, pp. 199–215. doi:10.1111/j.2153-3490.1972.tb01547.x.

[7] Swartz, B., and Wendroff, B., "The Relative Efficiency of Finite Difference and Finite Element Methods. I: Hyperbolic Problems and Splines," *SIAM Journal on Numerical Analysis*, Vol. 11, No. 5, 1974, pp. 979–993. doi:10.1137/0711076.

[8] Wang, Z. J., Fidkowski, K., Abgrall, R., Bassi, F., Caraeni, D., Cary, A., Deconinck, H., Hartmann, R., Hillewaert, K., Huynh, H. T., et al., "High-Order CFD Methods: Current Status and Perspective," *International Journal for Numerical Methods in Fluids*, Vol. 72, No. 8, 2013, pp. 811–845.

[9] Zingg, D. W., "Comparison of High-Accuracy Finite-Difference Methods for Linear Wave Propagation," *SIAM Journal on Scientific Computing*, Vol. 22, No. 2, 2000, pp. 476–502. doi:10.1137/S1064827599350320.

[10] Del Rey Fernández, D. C., Boom, P. D., and Zingg, D. W., "A Generalized Framework for Nodal First Derivative Summation-by-Parts Operators," *Journal of Computational Physics*, Vol. 266, 2014, pp. 214–239.

[11] Nordström, J., and Carpenter, M. H., "High-Order Finite Difference Methods, Multidimensional Linear Problems, and Curvilinear Coordinates," *Journal of Computational Physics*, Vol. 173, No. 1, 2001, pp. 149–174. doi:10.1006/jcph.2001.6864.

[12] Hicken, J. E., and Zingg, D. W., "Parallel Newton-Krylov Solver for the Euler Equations Discretized Using Simultaneous Approximation Terms," *AIAA Journal*, Vol. 46, No. 11, 2008, pp. 2773–2786. doi:10.2514/1.34810.

[13] Hicken, J. E., Del Rey Fernández, D. C., and Zingg, D. W., "Multidimensional Summation-by-Parts Operators: General Theory and Application to Simplex Elements," *SIAM Journal on Scientific Computing*, Vol. 38, No. 4, 2016, pp. A1935–A1958. doi:10.1137/15M1038360.

[14] Del Rey Fernández, D. C., Hicken, J. E., and Zingg, D. W., "Simultaneous Approximation Terms for Multi-Dimensional Summation-by-Parts Operators," *Journal of Scientific Computing*, Vol. 75, No. 1, 2018, pp. 83–110. doi:10.1007/s10915-017-0523-7.

[15] Hicken, J. E., and Zingg, D. W., "Summation-by-Parts Operators and High-Order Quadrature," *Journal of Computational and Applied Mathematics*, Vol. 237, No. 1, 2013, pp. 111–125. doi:10.1016/j.cam.2012.07.015.

[16] Chapra, S. C., and Canale, R. P., *Numerical Methods for Engineers*, seventh edition ed., McGraw-Hill Education, New York, NY, 2015.

[17] Liu, Y., and Vinokur, M., "Exact Integrations of Polynomials and Symmetric Quadrature Formulas over Arbitrary Polyhedral Grids," *Journal of Computational Physics*, Vol. 140, 1998, pp. 122–147.

[18] Taylor, M. A., Wingate, B. A., and Bos, L. P., "A Cardinal Function Algorithm for Computing Multivariate Quadrature Points," *SIAM Journal on Numerical Analysis*, Vol. 45, No. 1, 2007, pp. 193–205. doi:10.1137/050625801.

[19] Williams, D. M., Shunn, L., and Jameson, A., "Symmetric Quadrature Rules for Simplexes Based on Sphere Close Packed Lattice Arrangements," *Journal of Computational and Applied Mathematics*, Vol. 266, 2014, pp. 18–38. doi:10.1016/j.cam.2014.01.007.

[20] Witherden, F. D., and Vincent, P. E., "On the Identification of Symmetric Quadrature Rules for Finite Element Methods," *Computers & Mathematics with Applications*, Vol. 69, No. 10, 2015, pp. 1232–1241. doi:10.1016/j.camwa.2015.03.017.

[21] Zhang, L., Cui, T., and Liu, H., "A Set of Symmetric Quadrature Rules on Triangles and Tetrahedra," *Journal of Computational Mathematics*, Vol. 27, No. 1, 2009, pp. 89–96.

[22] Ibrahimoglu, B. A., "Lebesgue Functions and Lebesgue Constants in Polynomial Interpolation," *Journal of Inequalities and Applications*, Vol. 93, 2016. doi:10.1186/s13660-016-1030-3.

[23] Blyth, M. G., Luo, H., and Pozrikidis, C., "A Comparison of Interpolation Grids over the Triangle or the Tetrahedron," *Journal of Engineering Mathematics*, Vol. 56, No. 3, 2007, pp. 263–272. doi:10.1007/s10665-006-9063-0.

[24] Witherden, F. D., and Vincent, P. E., "An Analysis of Solution Point Coordinates for Flux Reconstruction Schemes on Triangular Elements," *Journal of Scientific Computing*, Vol. 61, No. 2, 2014, pp. 398–423. doi:10.1007/s10915-014-9832-2.

[25] Witherden, F. D., Park, J. S., and Vincent, P. E., "An Analysis of Solution Point Coordinates for Flux Reconstruction Schemes on Tetrahedral Elements," *Journal of Scientific Computing*, Vol. 69, No. 2, 2016, pp. 905–920. doi:10.1007/s10915-016-0204-y.

[26] Diener, P., Dorband, E. N., Schnetter, E., and Tiglio, M., "Optimized High-Order Derivative and Dissipation Operators Satisfying Summation by Parts, and Applications in Three-Dimensional Multi-Block Evolutions," *Journal of Scientific Computing*, Vol. 32, No. 1, 2007, pp. 109–145.

[27] Mattsson, K., Almquist, M., and Carpenter, M. H., "Optimal Diagonal-Norm SBP Operators," *Journal of Computational Physics*, Vol. 264, 2014, pp. 91–111.

[28] Bos, L., "On Certain Configurations of Points in Rn Which Are Unisolvent for Polynomial Interpolation," *Journal of Approximation Theory*, Vol. 64, 1991, pp. 271–280.

[29] Hesthaven, J. S., and Warburton, T., *Nodal Discontinuous Galerkin Methods: Algorithms, Analysis, and Applications*, No. 54 in Texts in Applied Mathematics, Springer, New York, 2008. OCLC: ocn191889938.

[30] Chen, T., and Shu, C.-W., "Entropy Stable High Order Discontinuous Galerkin Methods with Suitable Quadrature Rules for Hyperbolic Conservation Laws," *Journal of Computational Physics*, Vol. 345, 2017, pp. 427–461. doi:10.1016/j.jcp.2017.05.025.

[31] Del Rey Fernández, D., Crean, J., Carpenter, M., and Hicken, J., "Staggered-Grid Entropy-Stable Multidimensional Summation-by-Parts Discretizations on Curvilinear Coordinates," *Journal of Computational Physics (accepted)*, 2019. doi:10.1016/j.jcp.2019.04.029.

[32] Derzko, N., and Pfeffer, A., "Bounds for the Spectral Radius of a Matrix," *Mathematics of Computation*, Vol. 19, No. 89, 1965, pp. 62–67.

[33] Hicken, J. E., Del Rey Fernández, D. C., and Zingg, D. W., "Opportunities for Efficient High-Order Methods Based on the Summation-by-Parts Property," *AIAA 2015-3198*, American Institute of Aeronautics and Astronautics, Dallas, Texas, 2015. doi:10.2514/6.2015-3198.

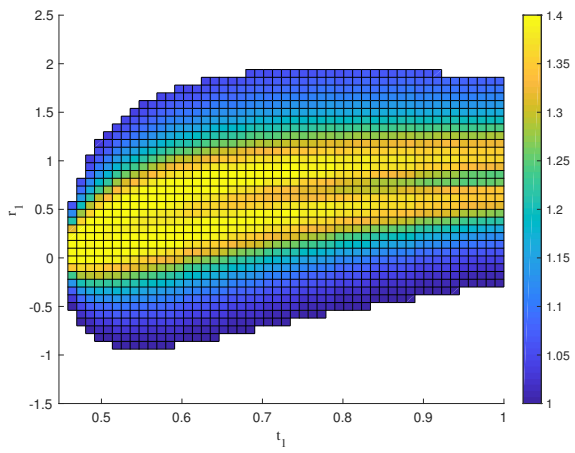

(a) Normalized solution error

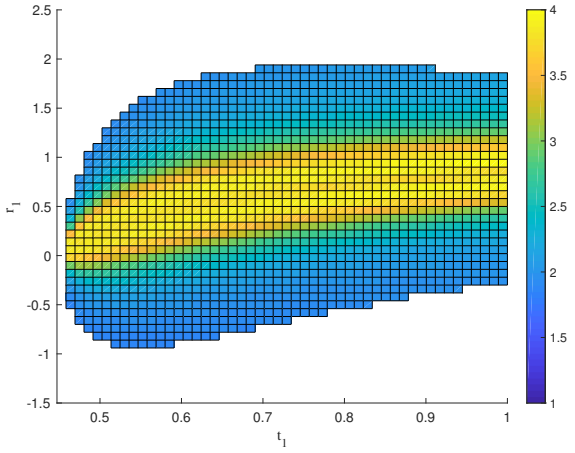

(b) Normalized dissipation of the kinetic energy

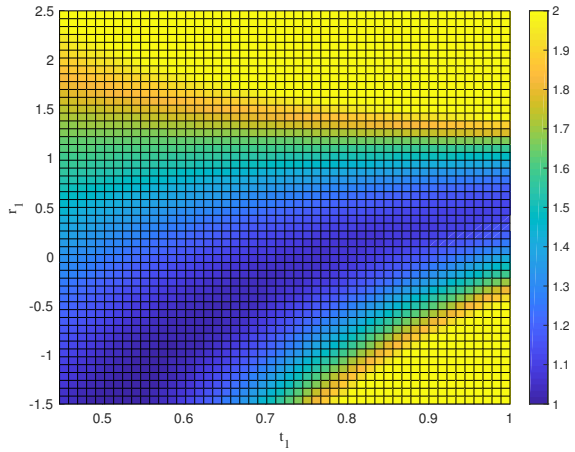

(c) Normalized facet integration error

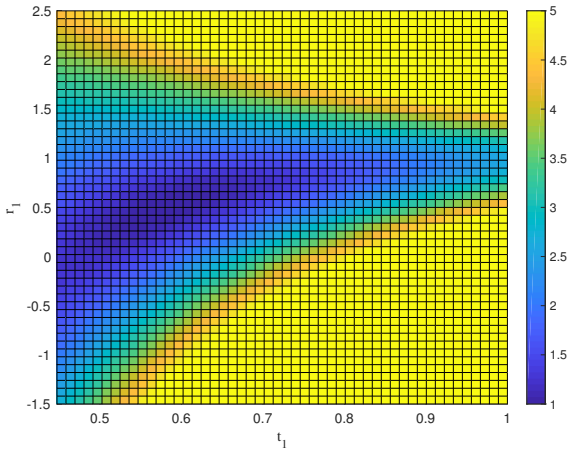

(d) Normalized interpolation/extrapolation error

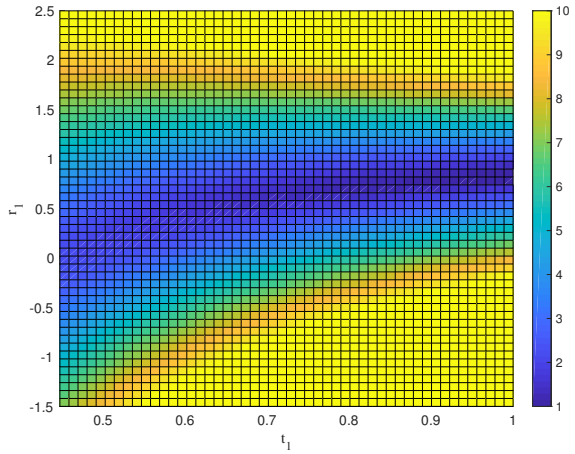

(e) Normalized Frobenius norm of D_ξ

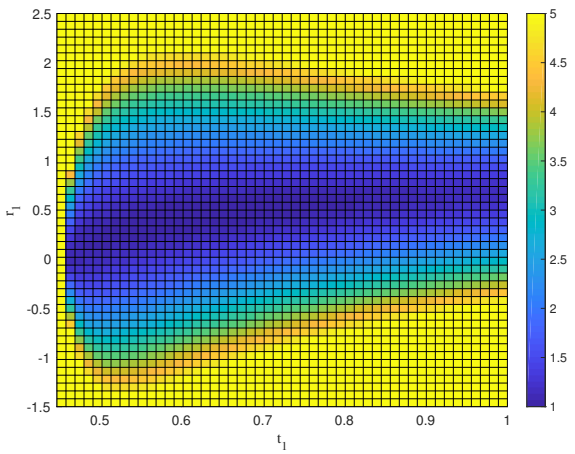

(f) Normalized Frobenius norm of A

Fig. 6 Solution error, dissipation in kinetic energy and objective function for $p = 1$ Ω tetrahedral operator with five nodes (s_{cent} and one $s_{c\text{-}vert}$ symmetry groups) and $p_{cub} = 2$.

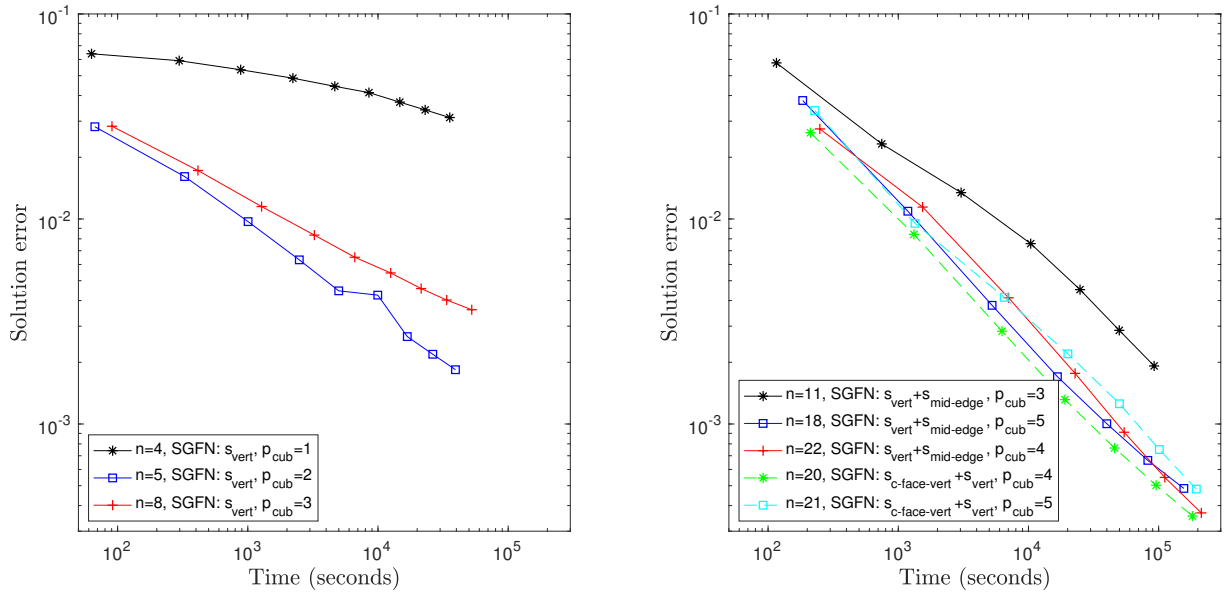

(a) $p = 1$ **(b)** $p = 2$ **with CFL =** 0.01

Fig. 7 Solution error and computational cost for Γ operators on tetrahedral elements, where SGFN stands for symmetry groups with facet nodes.

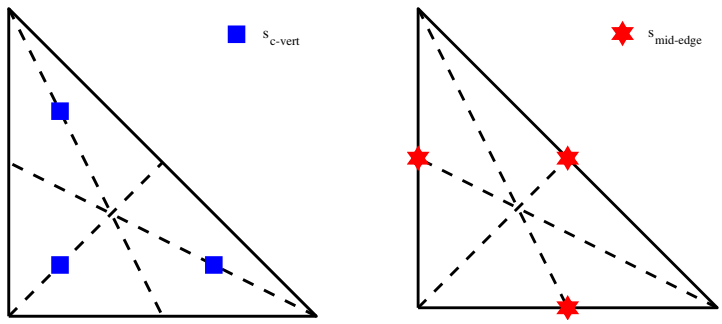

(a) $s_{\text{c-vert}}$ **symmetry group** **(b)** $s_{\text{mid-edge}}$ **symmetry group**

Fig. 8 Cubature rules of degree two on triangles used for $p = 1$ diagonal-E operators on tetrahedral elements

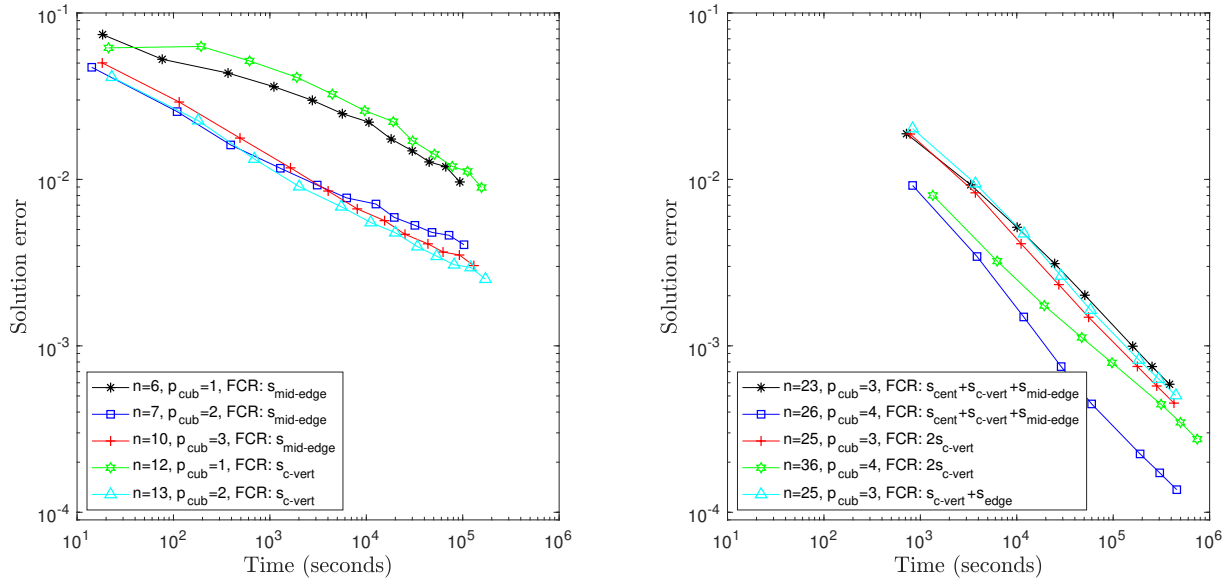

(a) $p = 1$ **(b)** $p = 2$

Fig. 9 Solution error and computational cost for diagonal-E operators on tetrahedral elements, where FCR stands for facet cubature rule.

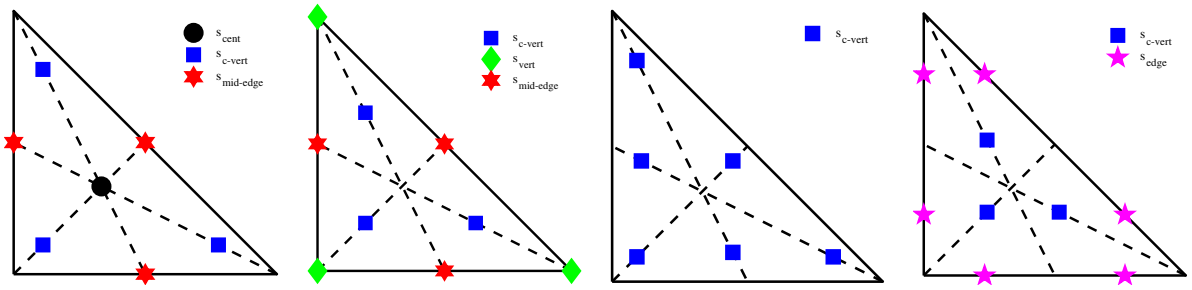

(a) ID: 3 **(b) ID: 5** **(c) ID: 7** **(d) ID: 8**

Fig. 10 Cubature rules of degree four on triangles from Table 8 used for $p = 2$ diagonal-E operators on tetrahedral elements.